

Multimodality Medical Image Fusion Based on New Features in NSST Domain

Padma Ganasala and Vinod Kumar

Received: 30 July 2014 / Revised: 30 November 2014 / Accepted: 4 December 2014
© The Korean Society of Medical & Biological Engineering and Springer 2014

Abstract

Purpose Multimodality medical image fusion supports better visualization of complimentary information given by different medical imaging modalities. This helps the radiologist for the precise diagnosis of disease and treatment planning. Main purpose of this research is to design a unified framework for fusion of different anatomical imaging modalities and fusion of functional image with an anatomical image.

Methods A novel image fusion framework utilizing new features in Nonsubsampled Shearlet Transform (NSST) domain is proposed for fusion of anatomical images. The source images are represented in low-frequency (LF) and high-frequency (HF) sub-bands using NSST. LF sub-bands are combined by fusion rule based on sum of variation in squares. HF fusion rule is formulated based on two different features. Inverse NSST of fused sub-bands gives the fused image. Further, this framework is utilized for fusion of functional and anatomical images in l-Alpha-Beta color space.

Results The proposed image fusion framework is validated on nine sets of CT-MRI, and SPECT-MRI images of different diseases. It is compared with state of the art image fusion methods both quantitatively and qualitatively.

Conclusions Visual analysis of CT-MRI image fusion results reveal that the fused images by proposed method retain the salient information of both CT and MRI images with more contrast than other methods. Fused SPECT-MRI images by proposed method presents anatomical details of MRI images without altering the functional content of SPECT images. However, spectral distortion is present in other methods. Quantitative comparison proved the superiority proposed method compared to other methods.

Keywords Image fusion, Nonsubsampled shearlet transform, l-alpha-beta color space, MRI-PET fusion, CT-MRI fusion

INTRODUCTION

There are different medical imaging modalities each giving the specific information about the human body. These are classified into two categories: anatomical imaging modalities and functional imaging modalities. The examples of anatomical imaging modalities are X-ray Computed Tomography (CT), Magnetic Resonance Imaging (MRI) T1, T2 sequences, and Ultrasonography. In specific, CT images provide the electron density map required for accurate dose calculation in radiotherapy treatment planning and superior hard tissue contrast. However, they are limited in soft tissue contrast, which is required for differentiating diseased tissues and normal tissues in different parts of the body. MRI provides excellent soft tissue contrast, but it has no signal from cortical bone. A fusion of these two anatomical imaging modalities allows better visualization all types of tissues. CT and MR image fusion is used to improve lesion delineation for radiation therapy planning, prostate seed implant quality analysis, planning the correct surgical procedure in computer-assisted navigated neurosurgery of temporal bone tumors [1], and orbital tumors [2]. Functional imaging modalities like Positron Emission Tomography (PET) and Single Photon Emission Computed Tomography (SPECT) provide important information about functionality of tissues and metabolic rate of tumors. However, it is difficult for nuclear physician to interpret these functional images without anatomical context. Image fusion permits the functional information given by PET or SPECT images to combine with the anatomical information given by CT or MRI image. Fusion image of PET/SPECT with CT/MRI is quite useful for differentiation between lesions and normal structures, the diagnosis of recurrent

Padma Ganasala (✉), Vinod Kumar
Department of Electrical Engineering, Indian Institute of Technology
Roorkee, Roorkee, Uttarakhand, 247667, India
Tel : +91-1332-286381 / Fax : +91-1332-276351
E-mail : Padma_417@yahoo.co.in

tumors, and for better radiotherapy treatment planning of head-and-neck cancers. Multimodality image fusion had a pivotal role in the assessment of central nervous system disorders such as seizures, Alzheimer's disease, Parkinson's disease, head injury, and inoperable brain tumors [3]. The main objective of the present work is to design an innovative multimodality medical image method, which is useful for radiologist and nuclear physician in making the diagnosis as well as for treatment planning.

Aforementioned potential applications of multi-modality medical image fusion attracted the attention of many researchers worldwide. There are various image fusion strategies proposed by researchers to achieve the optimum fusion results. These methods are categorised as spatial domain image fusion methods, morphological operators based, neural network based, fuzzy logic based, and multi-scale decomposition (MSD) transform based image fusion methods. Few researchers also have combined two strategies together like neural networks in transform domain and fuzzy logic in the transform domain. Spatial domain image fusion methods include simple averaging or weighted averaging based on pixel saliency, principle component analysis based method, and robust principle component analysis [4] based methods. Spatial domain averaging methods suffer from reduction in contrast eventually loss of few details of source images. However, they have less computational complexity. Xiangzhi Bai *et al.* [5] proposed image fusion based on multi-scale top hat transform [6]. However, the results of these morphological operators based image fusion methods are sensitive to the structuring element used. The type of neural networks used for image fusion applications is Pulse Coupled Neural Network (PCNN) based on cat's visual cortex [7]. The major concern of PCNN based methods is setting the value for more number of parameters and increased computational complexity. Modified version of PCNN: dual channel PCNN, Intersecting Cortical Model(ICM), and Spiking Cortical Model (SCM) are also applied for image fusion [8]. The fuzzy logic based image fusion algorithms uses fuzzy implication operations [9]. The final fusion outcome depends on selection of membership functions and fuzzy sets.

The most widely researched image fusion category is Multi-scale Decomposition transform (MSD) based image fusion methodology which is commonly known as transform domain image fusion. The main philosophy of transform domain image fusion is the decomposition of source images using MSD transform, fusion of the resulting coefficients by means of different fusion rules, and then reconstructing the fused image through inverse MSD transform. Here the interesting factors are the choice of MSD transform and fusion rules. Various MSD transforms: wavelets[10], curvelets [11], contourlets [12], bandlets [13], framelets [14], and

shearlets [15] are tested for image fusion application. Among them wavelets have limited directional capability and all of them have common drawback of shift variance which causes blocking artefacts around the singularities. Finally, the shift invariant MSD transforms: Nonsampled Contourlet Transform (NSCT) [16] and Nonsampled Shearlet Transform (NSST) [17, 18] proved to be promising for image fusion. As mentioned, another factor that has greater impact on the quality of fused image in MSD transform based image fusion algorithm is fusion rule used for combining coefficients after decomposition. The fusion rules that have been tested so far come under two categories: fusion rules based on coefficient saliency measures and fusion rules based on neural networks. Bhatnagar [19] used Phase congruency and directive contrast in NSCT domain. Regional energy, regional energy contrast, regional clarity contrast, and regional variance contrast are adapted in [20] to fuse coefficients in NSCT domain. Improved non-negative matrix factorization and contrast are employed to fuse NSST coefficients in [21]. The NSST based method utilizing non-classic-RF is proposed in [22]. Energy and contrast based fusion rules are used in NSST domain [23]. PCNN based fusion rules in NSCT domain is adapted in [24]. Dual channel PCNN and NSCT are used in [25]. Modified spatial frequency driven PCNN based fusion rules are proposed in [26]. Simplified PCNN model called improved intersecting cortical model (I2CM) based fusion rule is adapted in [27]. Weiwei Kong proposed Improved PCNN based fusion rules which adapts contrast as linking strength [28] and spatial frequency as linking strength [29] in NSST domain. PCNN based fusion showed good performance at the cost of increased computational complexity. Even though, fusion rules in MSD transform domain are greatly explored, there is a further scope to improve the image fusion quality by modifying the fusion rules in NSST domain. This inspired us to propose a new image fusion methodology in NSST domain that is superior to the current methods for multimodality medical images.

Fusion of functional image with an anatomical image is dealt in a slightly different way because the functional image is a pseudo color image whereas the anatomical image is a gray scale image. In this process, it is very important to retain the color of functional image and the spatial details of anatomical image. Any change in color of fused image compared to source functional image is known as spectral distortion and any loss of spatial details of fused image as compared to anatomical image is known as spatial distortion. Baum KG *et al.* proposed fusion viewer based on color tables [30, 31]. In these methods, the fused image is not similar to source images because of using color tables. Image fusion methods based on color models or color spaces take

major role in functional and anatomical image fusion. Two types of Intensity, Hue, and Saturation (IHS) color models called linear and nonlinear IHS color models are widely used in the literature for functional- anatomical image fusion. In IHS based method [32] simply intensity component (I) is replaced with anatomical image which resulted in spectral distortion. In IHS and PCA method [33], PCA is used to combine I and anatomical image. This method also has spectral distortion problem. In [34], retina inspired models are used to combine I and anatomical image. The hybrid intelligent system is used in [9]. Another direction to improve the spatial and spectral quality is by using MSD transform based image fusion method in a better color model.

In the present work, we proposed a novel NSST based image fusion algorithm to fuse the two anatomical images. The same is extended for fusion functional and anatomical images in l-Alpha-Beta ($l\alpha\beta$) color space. The reason for using $l\alpha\beta$ color space is that it has better de-correlation of intensity channel from chromatic channels. This reduces the effect of fusion in its intensity channel on the chromatic content. Hence, it is possible to reduce the spectral distortion.

PROPOSED MULTIMODALITY MEDICAL IMAGE FUSION FRAMEWORK

The proposed anatomical image fusion framework is described in section 2.1 and the functional-anatomical image fusion is described in section 2.2.

Anatomical image fusion framework

In the proposed image fusion method, a shift invariant multi-scale and multi-direction decomposition transform NSST is used. More details of NSST available in [17]. The schematic of proposed anatomical image fusion framework is shown in Fig. 1. The source images A and B are transformed into low-frequency (LF) and band-pass directional sub-bands or high-frequency (HF) sub-bands by using NSST. Then LF sub-bands are combined by using LF sub-band fusion rule based on novel feature inspired by human visual system as described in the following subsection 2.1.1. The HF sub-bands are fused by using HF sub-band fusion rule based on two activity level measurement parameters as described in the following subsection 2.1.2 Finally, the fused image is reconstructed through inverse NSST of fused sub-bands.

LF sub-band fusion rule

As the LF sub-band represents the overall outline of the image, it is intuitive to use Human visual system (HVS) inspired feature in low-frequency sub-band fusion rule. HVS is sensitive to local variations in the image instead of the absolute luminance value of the image. Most of the signal

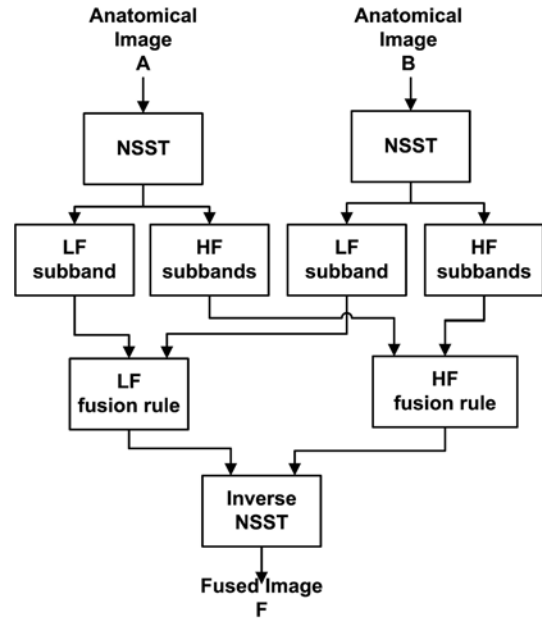


Fig. 1. Schematic of proposed NSST based image fusion method for anatomical images.

energy is present in the LF sub-band of the image. Based on these two facts, saliency metric of LF sub-band coefficient is formulated as the sum of variation in the squares of the coefficients. The calculation of this saliency metric is described in the following steps:

Let $f(x, y)$ be any function. The variation in the square of the function is given by the following equation:

$$lv[f(x, y)] = \sum_{m=-1}^1 \sum_{n=-1}^1 |(f(x, y))^2 - f(x+m, y+n)^2| \tag{1}$$

Sum of local variation is defined as

$$slv[f(x, y)] = \sum_{i=-1}^1 \sum_{j=-1}^1 w(i+1, j+i)lv[f(x+i, y+j)] \tag{2}$$

$$w = \frac{1}{16} \begin{bmatrix} 1 & 2 & 1 \\ 2 & 4 & 2 \\ 1 & 2 & 1 \end{bmatrix} \tag{3}$$

Consider LF sub-band coefficients of source images A and B as $C_L^A(i, j)$, and $C_L^B(i, j)$ respectively. Now, the saliency $a_L^A(i, j)$ and $a_L^B(i, j)$ of $C_L^A(i, j)$ and $C_L^B(i, j)$ is obtained by using Eqs. (1) and (2).

$$a_L^A(i, j) = slv[C_L^A(i, j)] \tag{4}$$

$$a_L^B(i, j) = slv[C_L^B(i, j)] \tag{5}$$

Now, the initial fusion decision map is obtained as:

$$d(i, j) = \begin{cases} 1 & \text{if } a_L^A(i, j) \geq a_L^B(i, j) \\ 0 & \text{if } a_L^A(i, j) < a_L^B(i, j) \end{cases} \quad (6)$$

To maintain the consistency in coefficient selection, initial fusion decision map is subject to morphological opening and closing operation with structuring element (SE) having square shape. The opening operation removes the stray background pixels of initial decision map d . Followed by closing remove the holes in the foreground. This process allows the uniformity in the selection of coefficients.

$$df = (d \circ SE) \bullet SE \quad (7)$$

Fused LF sub-band coefficients $C_L^F(i, j)$ are calculated by using the final decision map df .

$$C_L^F(i, j) = \begin{cases} C_L^A(i, j) & \text{if } df(i, j) = 1 \\ C_L^B(i, j) & \text{if } df(i, j) = 0 \end{cases} \quad (8)$$

HF sub-band fusion rule

HF sub-band coefficients represent details or edges present in the source images. HF sub-band coefficients corresponding to edge locations have more amplitude compared to non-edge locations. HVS is sensitive to edges and it is able to perceive the edges by exaggerating the contrast between the edges of slightly different gray shades. Hence, in the proposed method, two activity level measurement parameters: absolute maximum within a 3×3 neighbourhood and the sum of absolute differences of successive rows and columns within a 3×3 neighbourhood are utilised in the high frequency fusion rule. First one represents the dominant edges present in the source image and the second one represent the contrast between the edges. At each location of high frequency sub-bands, these two activity level measurement parameters are calculated as follows:

Let $C_{d,k}^A(i, j)$, and $C_{d,k}^B(i, j)$ are the d^{th} scale, K^{th} directional subband coefficients of image A , and B at location (i, j) respectively. Then, the first activity level measurement parameter is given by:

$$a1_{d,k}^A(i, j) = \max_{-1 \leq m \leq 1, -1 \leq n \leq 1} |C_{d,k}^A(i+m, j+n)| \quad (9)$$

The second activity level measurement parameter is defined as:

$$\begin{aligned} a2_{d,k}^A(i, j) = & \sum_{m=-1}^1 abs(C_{d,k}^A(i+m, j) - C_{d,k}^A(i+m, j+1)) \\ & + \sum_{m=-1}^1 abs(C_{d,k}^A(i+m, j) - C_{d,k}^A(i+m, j-1)) \\ & + \sum_{m=-1}^1 abs(C_{d,k}^A(i, j+m) - C_{d,k}^A(i+1, j+m)) \\ & + \sum_{m=-1}^1 abs(C_{d,k}^A(i, j+m) - C_{d,k}^A(i-1, j+m)) \end{aligned} \quad (10)$$

Similarly, two activity measurements $a1_{d,k}^B(i, j)$, $a2_{d,k}^B(i, j)$ of image B coefficient are calculated by using Eqs. (9) and (10). Fused image coefficient $C_{d,k}^F(i, j)$ is obtained as follows:

$$C_{d,k}^F(i, j) = \begin{cases} C_{d,k}^A(i, j) & \text{if } a1_{d,k}^A(i, j) > a1_{d,k}^B(i, j) \\ C_{d,k}^B(i, j) & \text{else if } a1_{d,k}^A(i, j) < a1_{d,k}^B(i, j) \\ C_{d,k}^A(i, j) & \text{else if } a2_{d,k}^A(i, j) > a2_{d,k}^B(i, j) \\ C_{d,k}^B(i, j) & \text{otherwise} \end{cases} \quad (11)$$

Functional and Anatomical image fusion framework

In fusion of functional image with an anatomical image, it is essential to inject all the spatial details of high-resolution gray scale anatomical image into the functional image without making any change to the color of the functional image. Hence, the first step is to convert a functional image into a color model in which achromatic information and chromatic information are represented in de-correlated channels. Next, fusion is performed in the achromatic channel of the functional image without disturbing its chromatic or color information content. Final fused image is obtained by converting new achromatic channel and two original chromatic channels into RGB format. Different authors have used IHS linear color model and IHS triangular model, etc. However, these color models could not perfectly de-correlate the achromatic and chromatic information or channels. Hence, image fusion performed using these color models may result in spectral distortion. In the proposed method, image fusion is performed in l-Alpha-Beta ($l\alpha\beta$) [35] color space which has better de-correlation property. As the functional image is originally in RGB format, it needs to be converted to $l\alpha\beta$ color space.

Conversion of RGB color space to $l\alpha\beta$ color space is described below:

Functional image originally represented in RGB format is converted to the LMS color space[36] which corresponds to human cone responses.

$$\begin{bmatrix} L \\ M \\ S \end{bmatrix} = \begin{bmatrix} 0.3811 & 0.5783 & 0.0402 \\ 0.1967 & 0.7244 & 0.0782 \\ 0.0241 & 0.1288 & 0.8444 \end{bmatrix} \begin{bmatrix} R \\ G \\ B \end{bmatrix} \quad (12)$$

Then LMS color space data is transformed to $l\alpha\beta$ color space by using the following transformation.

$$\begin{bmatrix} l \\ \alpha \\ \beta \end{bmatrix} = \begin{bmatrix} 1/\sqrt{3} & 0 & 0 \\ 0 & 1/\sqrt{6} & 0 \\ 0 & 0 & 1/\sqrt{2} \end{bmatrix} \begin{bmatrix} 1 & 1 & 1 \\ 1 & 1 & -2 \\ -1 & -1 & 0 \end{bmatrix} \begin{bmatrix} L \\ M \\ S \end{bmatrix} \quad (13)$$

The three axes in $l\alpha\beta$ color space are an achromatic direction or luminance channel (l), a yellow-blue opponent direction (α) and a red-green opponent direction (β). The author of $l\alpha\beta$ space suggested converting LMS color space into logarithmic space before converting to $l\alpha\beta$ space for natural images. However, in case of medical images this is making the dynamic range of luminance channel (l) quite different from that of the anatomical image and not yielding good fusion results. Hence, in the proposed method, LMS color space is converted $l\alpha\beta$ color space without converting to logarithmic space.

The conversion of $l\alpha\beta$ color space into RGB conversion is as follows:

Initially $l\alpha\beta$ color space is converted to LMS space by the following transformation.

$$\begin{bmatrix} L \\ M \\ S \end{bmatrix} = \begin{bmatrix} 1 & 1 & 1 \\ 1 & 1 & -1 \\ 1 & -2 & 0 \end{bmatrix} \begin{bmatrix} 1/\sqrt{3} & 0 & 0 \\ 0 & 1/\sqrt{6} & 0 \\ 0 & 0 & 1/\sqrt{2} \end{bmatrix} \begin{bmatrix} l \\ \alpha \\ \beta \end{bmatrix} \quad (14)$$

Then, LMS color model is converted to RGB format through following equation [36]

$$\begin{bmatrix} R \\ G \\ B \end{bmatrix} = \begin{bmatrix} 4.4679 & -3.5873 & 0.1193 \\ -1.2186 & 2.3809 & -0.1624 \\ 0.0497 & -0.2439 & 1.2045 \end{bmatrix} \begin{bmatrix} L \\ M \\ S \end{bmatrix} \quad (15)$$

The proposed functional and anatomical image fusion framework using $l\alpha\beta$ color space is shown in Fig. 2. The functional image, which is in RGB format, is converted to $l\alpha\beta$ color space. Then, the luminance component (l) is fused with anatomical image by using the proposed anatomical image fusion framework described in section 2.1 to get new luminance channel with all the details of anatomical image. Finally, this new fused luminance channel and original chromatic channels (α , and β) are converted to RGB format to obtain final fused image.

RESULTS AND DISCUSSIONS

For the validation of proposed anatomical image fusion framework, a set of nine CT and MRI (T2) images are used. These are acute stroke cases presenting as speech arrest, and writes, but cannot read, hypertensive Encephalopathy, multiple Infarcts, fatal stroke, metastatic bronchogenic carcinoma, meningioma, sarcoma, and cerebral toxoplasmosis cases. The first case is shown in Fig. 3 and the remaining cases are shown in Fig. 4. The proposed functional and anatomical image fusion framework is tested on SPECT and MRI (T2)

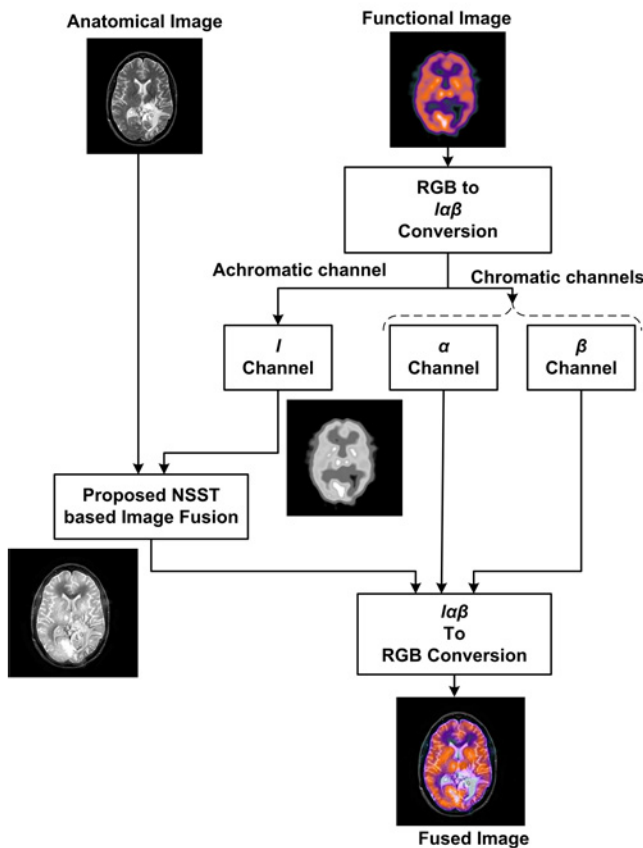


Fig. 2. Block diagram of proposed functional and anatomical image fusion framework.

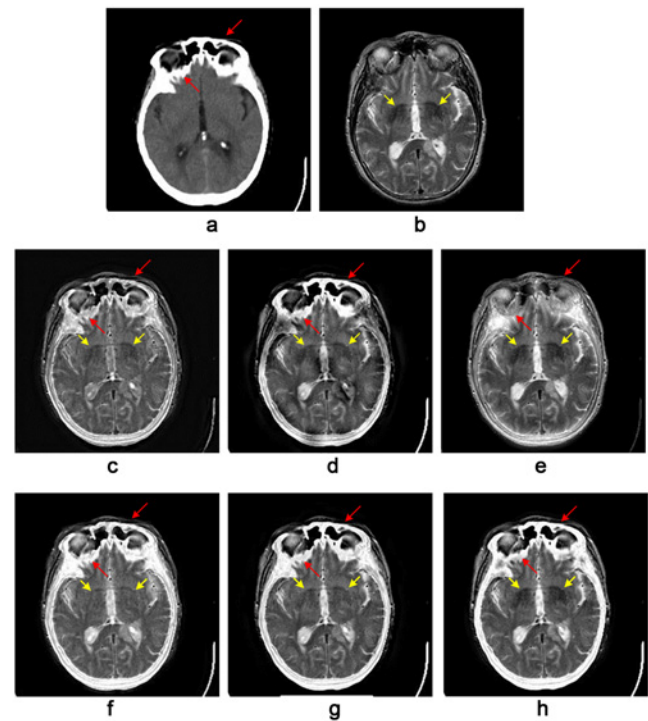


Fig. 3. (a) CT image, (b) MRI image, fused image by (c) M1 [22], (d) M2 [19], (e) M3 [27], (f) M4 [23], (g) M5 [20], and (h) M6.

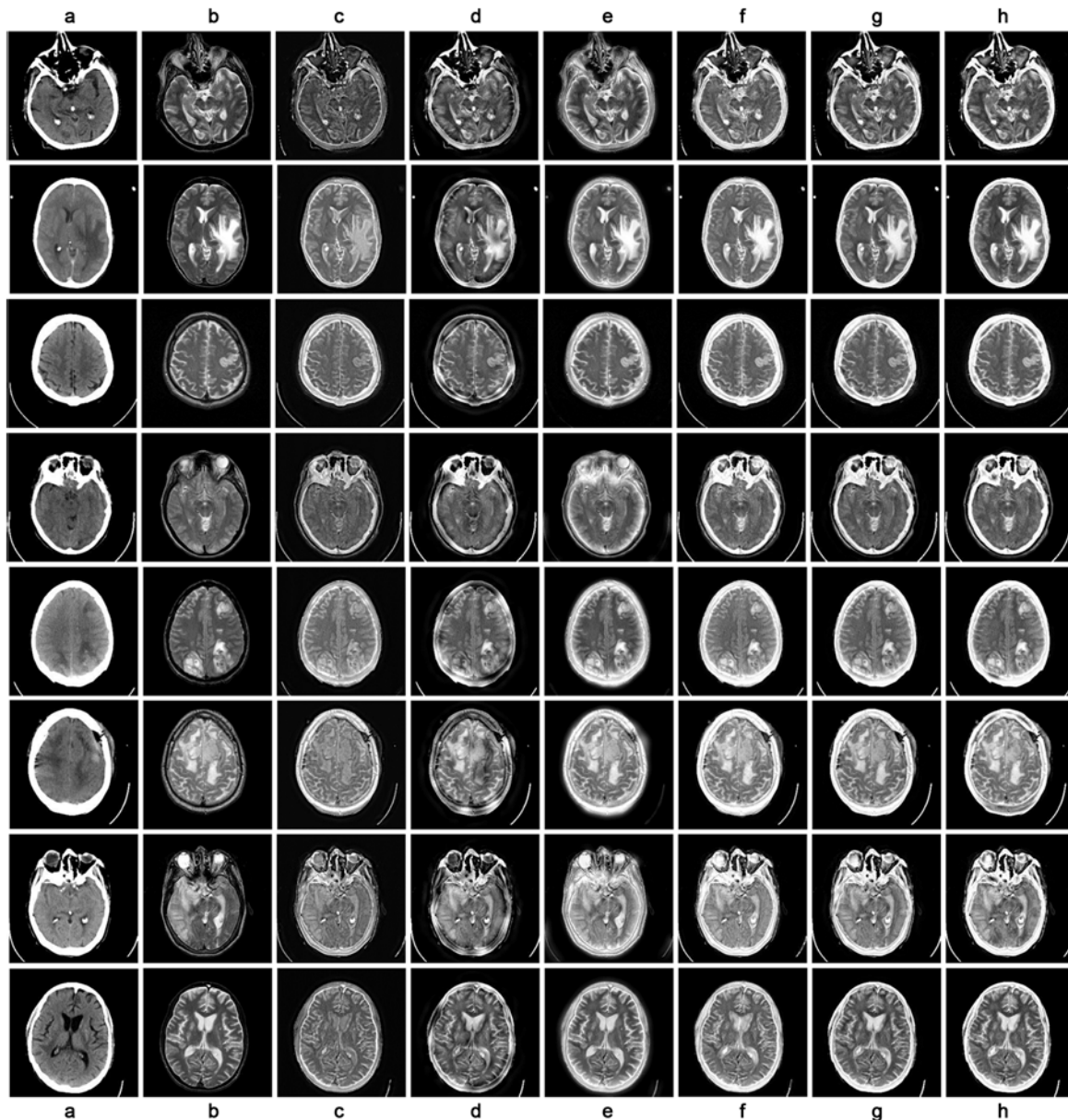


Fig. 4. (a) CT images, (b) MRI images, fused images by (c) M1 [22], (d) M2 [19], (e) M3 [27], (f) M4 [23], (g) M5 [20], and (h) M6.

images of nine different cases. These are cases are Anaplastic Astrocytoma, Sub-acute Stroke, Cavernous Haemangioma, Vascular Dementia, Hypertensive Encephalopathy, Astrocytoma, Mild Alzheimer's disease, Alzheimer's disease, and AIDS Dementia. These are shown in Figs. 6 and 7. Both CT/MRI and SPECT/MRI images are collected from <http://www.med.harvard.edu/aanlib/home.html>. All these images are made to be of same size 256×256 and are perfectly registered using superpose software tool. All the simulations are implemented in Matlab 2010b on a PC with Intel core 2 Duo, 3 GHz. This section emphasizes the following points: Methods used for comparison, CT-MRI image fusion results, SPECT-MRI image fusion results, and computational complexity comparison.

Methods used for comparison

The parameters of the proposed method are fixed as follows. The number decomposition levels of NSST are set to three. The numbers of directions from coarser scale to finer scale are fixed at four, eight, and eight. Accordingly, the shearing filter window width is set at 8, 16, and 16. There are no other thresholds or any variables to be adjusted in the proposed method and this is an advantage of the proposed method. From now on proposed method is denoted as the M6. In order to prove the impact of proposed anatomical image fusion method, it is compared with the following five latest methods. Fast non classic RF model based LF fusion rule and local directional contrast based HF fusion rule in NSST

domain [22] denoted as M1. The phase congruency based LF fusion rule and directive contrast based HF fusion rule in NSCT domain [19] denoted as M2. Improved intersecting cortical model based fusion rules in NSST domain [27] denoted as M3. Regional average energy based LF fusion rule and contrast based fusion HF fusion rule in NSST domain [23] denoted as M4. Weighted energy based LF fusion rule and neighbourhood characteristics based HF rule in NSCT [20] denoted as M5. The parameter setting and implementation of all these five methods are done as per the details given in the corresponding references.

In order to prove the significance of the proposed functional-anatomical image fusion method denoted as Method 6, it is compared with the following methods. IHS based method [32] denoted as Method1. NSCT based scheme [19] in $\alpha\beta$ color space denoted as Method2. NSST based schemes of [23, 27] in IHS color space denoted as Method3, and Method4 respectively. NSCT based scheme [20] in IHS color space denoted as Method5. This selection is to prove the suitability of used color model and proposed image fusion scheme for functional-anatomical image fusion.

CT-MRI image fusion results

The fused image of CT and MRI image must retain the bone details given by CT image and soft tissue details given by MRI image. Fused results of acute stroke case are shown in Fig. 3. The Globus pallidus structure present in the MRI image of this case is pointed with arrows in the Fig. 3b. This structure is having black shade in the original MRI image.

However, this appears as a gray shade in M1, M4, and M5. Hence, the soft tissue contrast in the fused images by these three methods is poor. The arrows shown in Fig. 3a represent the bone details in the CT image. However, there are a few discrepancies in the same bone structure to be present in the fused images by M2 and M3. This suggests that M2 and M3 methods are lacking in retaining the CT image information. By observing the fused image by proposing method M6 shown in Fig. 3h, it is clear that it has good contrast to Globus pallidus structure and there are no discrepancies in the bony details as well. Fused images of the remaining CT and MRI cases are shown in Fig. 4.

In addition to the visual analysis, quantitative comparison is also done on experimental results. The average value of each image fusion quality metric by considering the nine sets of CT and MRI images are shown in the graphs of Fig. 5. Comparison of image fusion methods with respect to Mutual information [37] based quality metric (MI) is shown in Fig. 5a. Mutual information between fused image and the source images are calculated and then added. This quality metric shows the similarity of fused image with the source images. If MI is large then image fusion quality is better. From the MI graph, it is clear that proposed method M6 is giving the higher value of MI compared to other methods. The quantitative comparison with respect to spatial frequency (SF) [37], and standard deviation (SD) of fused image are shown in Fig. 5b. The SF based quality metric gives the overall clarity of the fused image and SD gives the contrast of the fused image. The graph shown in Fig. 5b indicates that

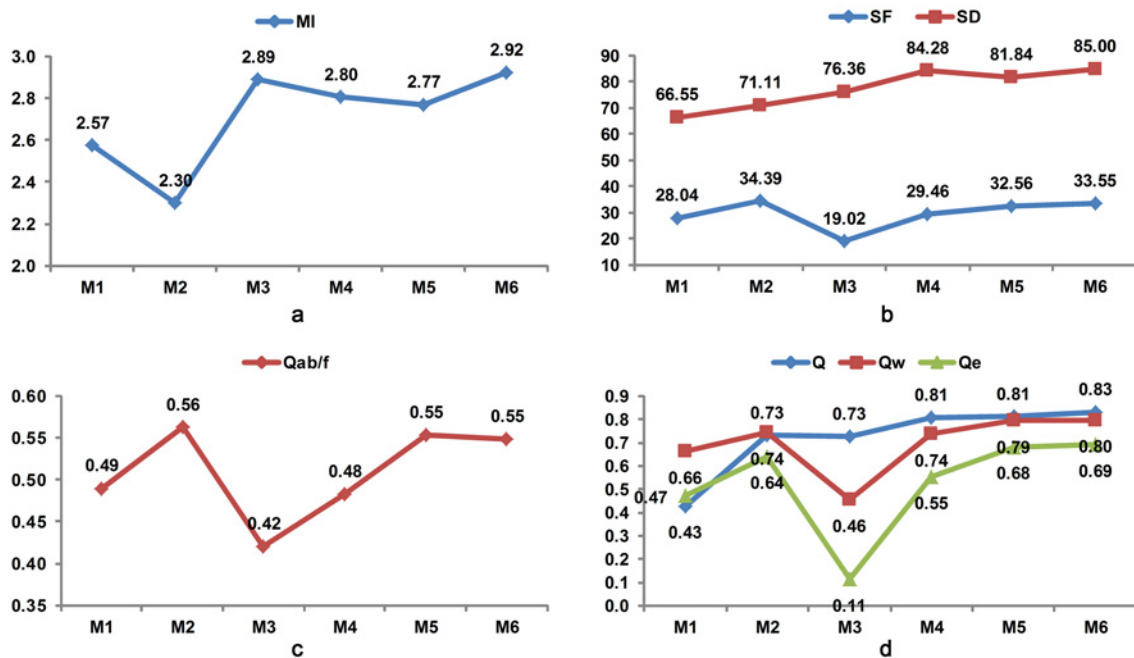


Fig. 5. Quantitative comparison of anatomical image fusion methods with respect to (a) Mutual Information (MI), (b) Spatial frequency (SF) and Standard deviation (STD), (c) Edge information based metric ($Q^{AB/F}$), and (d) UIQI based quality metrics Q , Q_w and Q_e .

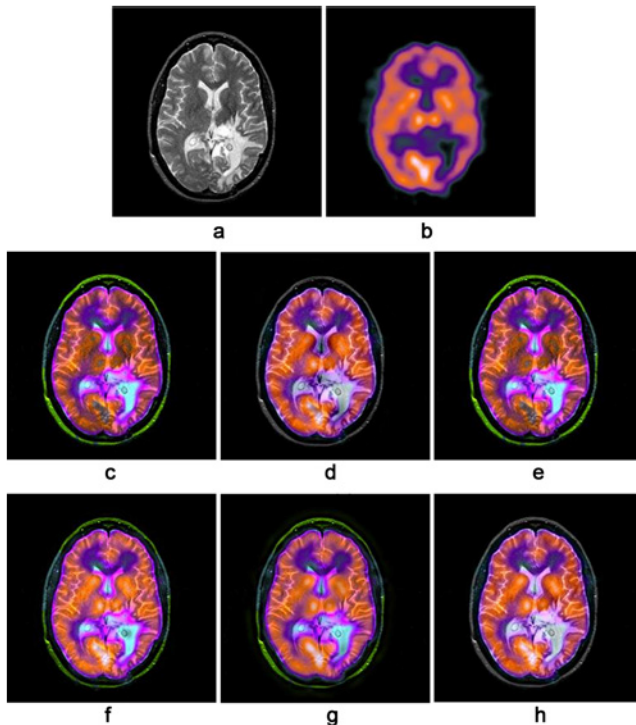


Fig. 6. (a) MRI image, (b) SPECT image, fused image by (c) Method1, (d) Method2, (e) Method3, (f) Method4, (g) Method5, and (h) Method6.

the SF values of M2 and the proposed method M6 are high compared to other methods. The SD is high for proposed method M6 compared to other methods. From the Fig. 5b, it is evident that the clarity and contrast of proposed method are better than other methods. The quantitative comparison with respect to edge information based quality metric proposed by Xydeas and Petrovic ($Q^{AB/F}$) [38] is shown in Fig. 5c. M2 method is showing slightly better performance with respect to this metric and that of the proposed method is almost equal to M2. Quantitative comparison with respect universal image quality index (UIQI) based image quality metrics (Q , Q_w and Q_c) proposed by G. Piella [39] is shown in Fig. 5d. These three image fusion quality measures (Q , Q_w and Q_c) have a dynamic range of [-1 1]. As the value of these quality metrics approaches one, image fusion quality increases. From the graphs shown in Fig. 5d, it is evident that the values of these three metrics given by proposed method are maximum compared to other methods. Hence, structural distortion is the minimum and the most of the salient information of source images is preserved in proposed method compared to other methods.

SPECT-MRI image fusion experimental results

The proposed functional and anatomical image fusion framework has been tested with SPECT and MRI brain images of nine different cases. SPECT images are in RGB

format and MRI images are in grayscale format. The fused image of MRI and SPECT must contain all the spatial details of high resolution MRI image and the color of fused image must be similar to that of low resolution SPECT image. Any loss in spatial detail compared to MRI and any change in the chromatic content of fused image compared to that of SPECT image are named as spatial distortion and spectral distortion respectively. The spectral distortion is a serious issue in functional-anatomical image fusion because this may leads to misdiagnosis and wrong treatment planning. The following observations have been made through visual analysis of SPECT-MRI experimental results shown in Figs. 6 and 7. The spectral distortion is less in case of Method 2 and Method 6. The regions where there is no uptake of radioactive tracer and high uptake areas in functional image are changed to different colors in case of remaining methods. This indicates that there is spectral distortion in Method 1, Method 3, Method 4 and Method 5 methods. In Method 5, we can observe blurred details also. The proposed method (Method 6) is preserving the details of MRI image without inherent spectral distortion.

In addition to visual analysis, quantitative comparison is done to quantify the spectral and spatial distortion incurred by different methods. The normalized mutual information (NMI), correlation coefficient (CC), and Bias are used to quantify the spectral distortion. Whereas, FCC and edge information based quality metric [38] ($Q_{ab/f}$) quantify the spatial distortion. The average of the each quality metric calculated for nine sets of SPECT and MRI images are shown in Fig. 8. NMI between each spectral band of fused image and the corresponding spectral band of the original functional image is calculated and then average is taken. The larger the value of NMI, the lesser is the spectral distortion. From the graph shown in Fig. 8a, it is evident that the NMI value of the proposed method (Method 6) is higher than that of all other methods and it is the minimum for Method 1. The CC between corresponding spectral bands of fused image and original functional image is calculated and then averaged over all spectral bands. The value of CC for different methods is shown in Fig. 8a. The Method 2 and Method 6 are giving highest CC value compared to other methods. Method1 is giving the lowest CC value. This implies that the spectral characteristic of Method 2 and Method 6 are better than other methods. Another spectral distortion quantifying metric, the Bias that is the average absolute difference between fused image spectral bands and the original functional image spectral bands over the mean value of the functional image spectral band is shown in Fig. 8b. It is important to note that the low value of bias indicates that the spectral distortion is less. From Fig. 8b, it is clear that the proposed method (Method 6) is giving the lower value of the bias compared to other methods. Hence,

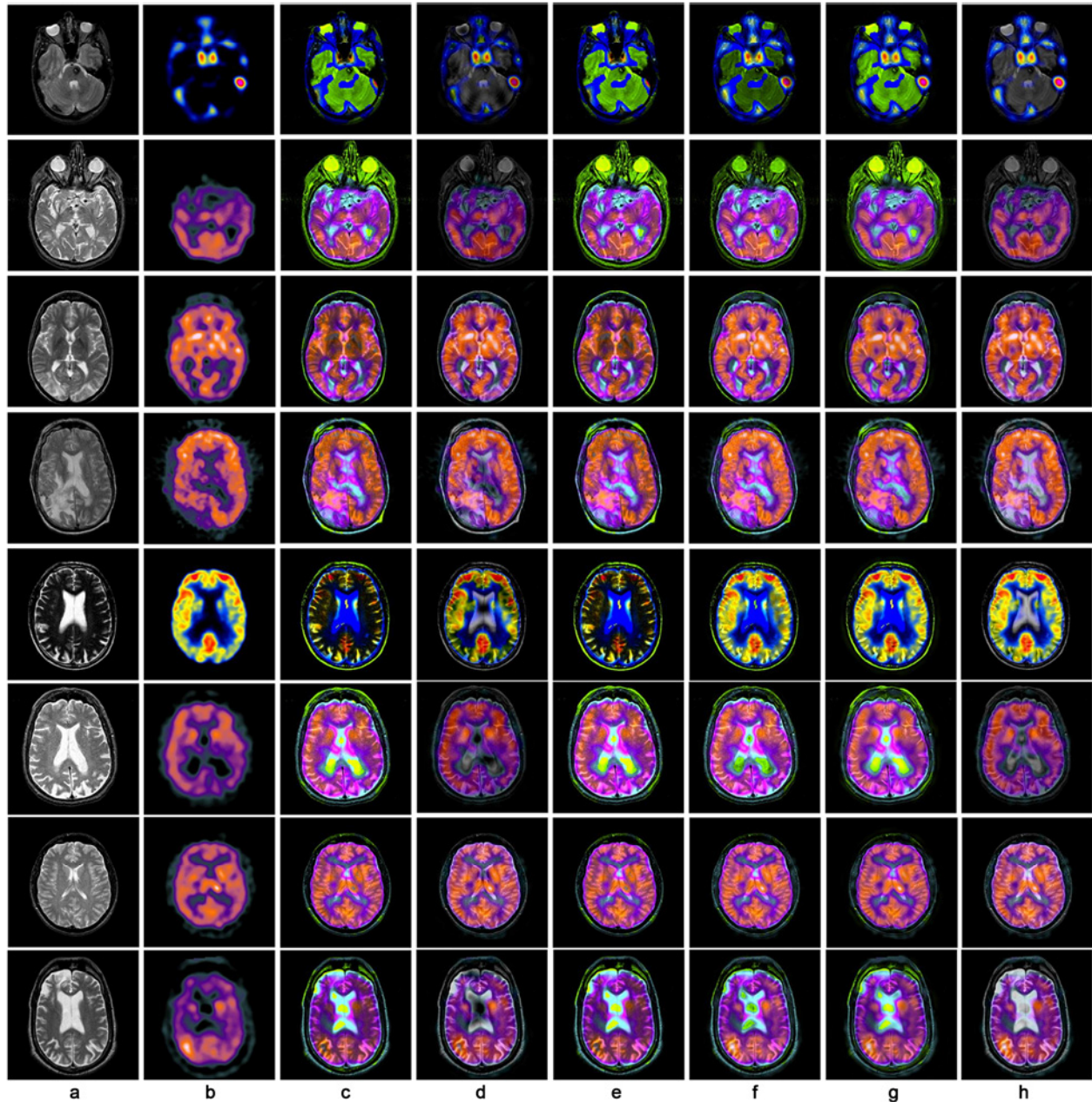


Fig. 7. (a) MRI images, (b) SPECT images, fused images by (c) Method1, (d) Method2, (e) Method3, (f) Method4, (g) Method5, and (h) Method6.

the three spectral distortion quantifying metrics proved that the spectral distortion is less in Method 6 compared to other methods. The FCC metric estimates the spatial distortion. The FCC is obtained in two steps: The original anatomical image and the fused image are filtered with Laplacian mask. Then, CC is calculated between each Laplacian filtered fused image spectral band and Laplacian filtered anatomical image spectral band and then averaged. The higher the value of FCC, the lesser is the spatial distortion. Comparison with respect to FCC is shown in Fig. 8c. FCC of the Method 6 is

slightly higher than other methods. FCC of the Method 5 is less than that of all other methods. Edge information based quality metric ($Q_{ab/f}$) is calculated between functional image, anatomical image, and fused image for each spectral band separately. Then the average is taken. Comparison with respect to this metric is shown in Fig. 8c. Method 1 is giving the least value of $Q_{ab/f}$. Whereas, $Q_{ab/f}$ value of Method 6 is higher. This implies that the spatial details of anatomical image are better preserved in the proposed method (Method 6) compared to other methods.

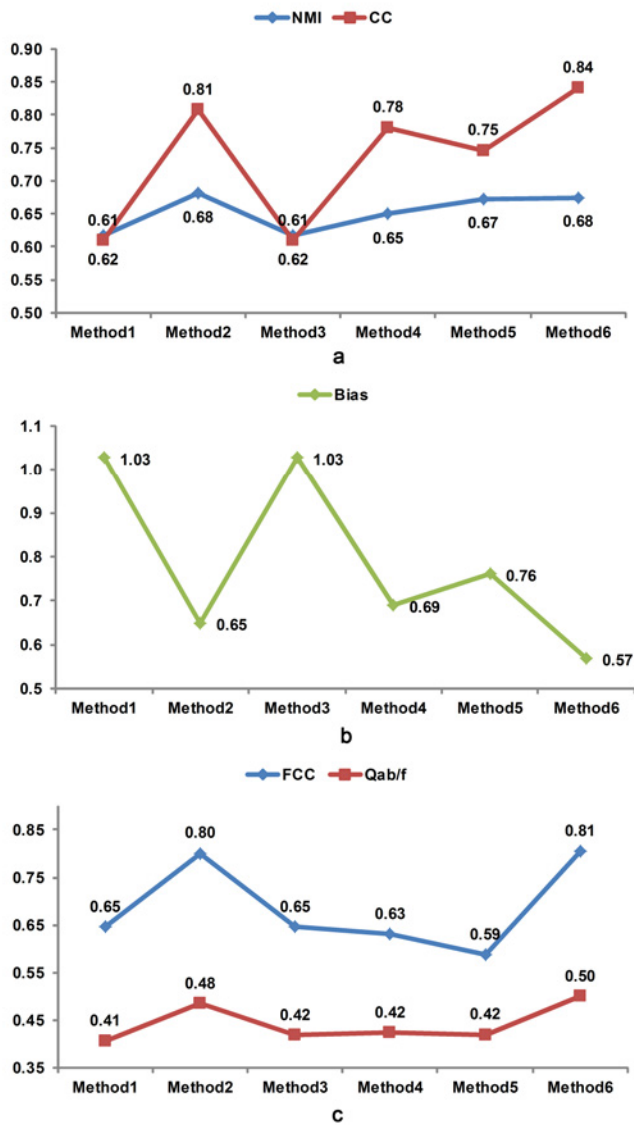


Fig. 8. Quantitative comparison of functional and anatomical image fusion methods with respect to (a) Normalised Mutual Information (NMI) and Correlation Coefficient (CC), (b) Bias, and (c) Filtered Correlation Coefficient (FCC) and Qab/f.

Computational complexity comparison

The running time of methods M1 to M6 for the image set shown in Fig. 3 is given in Table 1. Methods M1, M3, M4, and M6 are NSST based methods, whereas M2 and M5 are NSCT based methods. As NSCT is having higher computational complexity compared to NSST, the actual running times M2 and M5 are higher. M5 is taking highest time 304.58s, the reason being NSCT based method, and five regional features adapted in the method. M2 is taking second highest time 28.93s. M3 is taking third highest time 17.52s, because it uses neural network. M1 and M4 are taking less time 2.18s and 3.39s respectively. However, their

Table 1. Computational complexity comparison of different image fusion methods for CT-MRI dataset shown in Fig. 3.

	M1	M2	M3	M4	M5	M6
Time (s)	2.18	28.93	17.52	3.39	304.58	9.54

performance is poor. M6 is taking the moderate time 9.54s. Even though the time taken by M6 is higher than that of M1 and M4, its performance is better than all the methods compared in the present work which is proved through visual and quantitative analysis of experimental results.

CONCLUSIONS

In the present work, we proposed a novel multi-modality medical image fusion method based on new features in NSST domain. We used sum of variation in squares of coefficients in a neighbourhood for approximate sub-band fusion rule in order to preserve the energy and details of source images without introducing blocking artefacts into the fused image. Two features that are consistent with HVS are utilised for band-pass sub-band fusion rule to retain the edge information. We employed the l-alpha-beta color model, which has better de-correlation of achromatic and chromatic channels for functional and anatomical image fusion.

The proposed image fusion method is compared with latest methods based on NSCT and NSST quantitatively and qualitatively. We used nine sets of CT-MRI and SPECT-MRI for validation of the proposed method. Visual analysis of CT-MRI image fusion results reveal that fused images by proposed method contain bone details present in CT image and soft tissue details of MRI image with good contrast. However, other methods are lacking in retaining either CT or MRI information. Visual analysis of SPECT-MRI results shows that the fused images by proposed method retain anatomical details of MRI without altering the spectral content of functional image. In case of other methods, there is a change in the chromatic information in some regions. Quantitative analysis of experimental results in case of both CT-MRI image fusion and SPECT-MRI image fusion proved the superiority of the proposed scheme.

ACKNOWLEDGMENTS

We would like to thank anonymous reviewers and editor for their constructive comments which helped in improvement of the quality the paper. Also, we would like thank <http://www.med.harvard.edu/aanlib/home.html> for providing source medical images.

CONFLICT OF INTEREST STATEMENTS

Padma G declares that she has no conflict of interest in relation to the work in this article. Vinod K declares that he has no conflict of interest in relation to the work in this article.

REFERENCES

- [1] Nemeč SF, Donat MA, Mehraín S, Friedrich K, Krestan C, Matula C, Imhof H, Czerny C. CT–MR image data fusion for computer assisted navigated neurosurgery of temporal bone tumors. *Eur J Radiol*. 2007; 62(2):192–8.
- [2] Nemeč SF, Pelosček P, Schmook MT, Krestan CR, Hauff W, Matula C, Czerny C. CT–MR image data fusion for computer-assisted navigated surgery of orbital tumors. *Eur J Radiol*. 2010; 73(2):224–9.
- [3] Scott AM, Macapinlac H, Zhang JJ, Kalaigian H, Graham MC, Divgi CR, Sgouros G, Goldsmith SJ, Larson SM. Clinical applications of fusion imaging in oncology. *Nucl Med Biol*. 1994; 21(5):775–84.
- [4] Wan T, Zhu C, Qin Z. Multifocus image fusion based on robust principal component analysis. *Pattern Recogn Lett*. 2013; 34(9):1001–8.
- [5] Bai X, Zhou F. A unified form of multi-scale top-hat transform based algorithms for image processing. *Optik Int J Light Electron Opt*. 2013; 124(13):1614–9.
- [6] Bai X. Morphological image fusion using the extracted image regions and details based on multi-scale top-hat transform and toggle contrast operator. *Digit Signal Process*. 2013; 23(2):542–54.
- [7] Wang Z, Ma Y, Gu J. Multi-focus image fusion using PCNN. *Pattern Recogn*. 2010; 43(6):2003–16.
- [8] Wang Z, Ma Y, Cheng F, Yang L. Review of pulse-coupled neural networks. *Image Vision Comput*. 2010; 28(1):5–13.
- [9] Kavitha CT, Chellamuthu C. Medical image fusion based on hybrid intelligence. *Appl Soft Comput*. 2014; 20:83–94.
- [10] Li H, Manjunath BS, Mitra SK. Multisensor image fusion using the wavelet transform. *Graph Model Im Proc*. 1995; 57(3):235–45.
- [11] Ali FE, El-Dokany IM, Saad AA, Abd El-Samie FE-S. Curvelet fusion of MR and CT images. *Prog Electromagn Res C*. 2008; 3:215–24.
- [12] Yang L, Guo BL, Ni W. Multimodality medical image fusion based on multiscale geometric analysis of contourlet transform. *Neurocomputing*. 2008; 72(1–3):203–11.
- [13] Lu HM, Nakashima S, Li YJ, Zhang LF, Yang SY, Seiichi S. An improved method for CT/MRI image fusion on bandelets transform domain. *Appl Mech Mater*. 2012; 103:700–4.
- [14] Bhatnagar G, Jonathan Wu QM, Liu Z. Human visual system inspired multi-modal medical image fusion framework. *Expert Syst Appl*. 2013; 40(5):1708–20.
- [15] Miao Q-g, Shi C, Xu P-f, Yang M, Shi Y-b. A novel algorithm of image fusion using shearlets. *Optics Commun*. 2011; 284(6):1540–7.
- [16] da Cunha AL, Jianping Z, Do MN. The nonsubsampling contourlet transform: theory, design, and applications. *IEEE T Image Process*. 2006; 15(10):3089–101.
- [17] Easley G, Labate D, Lim W-Q. Sparse directional image representations using the discrete shearlet transform. *Appl Comput Harmon A*. 2008; 25(1):25–46.
- [18] Wang Q-L. Nonseparable shearlet transform. *IEEE T Image Process*. 2013; 22(5):2056–65.
- [19] Bhatnagar G, Wu QMJ, Zheng L. Directive contrast based multimodal medical image fusion in NSCT domain. *IEEE T Multimedia*. 2013; 15(5):1014–24.
- [20] Chen Y, Xiong J, Liu H-l, Fan Q. Fusion method of infrared and visible images based on neighborhood characteristic and regionalization in NSCT domain. *Optik Int J Light Electron Opt*. 2014; 125(17):4980–4.
- [21] Kong W. Technique for image fusion based on NSST domain INMF. *Optik Int J Light Electron Opt*. 2014; 125(11):2716–22.
- [22] Kong W, Liu J. Technique for image fusion based on NSST domain improved fast non-classical RF. *Infrared Phys Techn*. 2013; 61:27–36.
- [23] Kong W. Technique for gray-scale visual light and infrared image fusion based on non-subsampling shearlet transform. *Infrared Phys Techn*. 2014; 63:110–8.
- [24] Qu X-B, Yan J-W, Xiao H-Z, Zhu Z-Q. Image fusion algorithm based on spatial frequency-motivated pulse coupled neural networks in nonsubsampling contourlet transform domain. *Acta Automatica Sinica*. 2008; 34(12):1508–14.
- [25] Baohua Z, Xiaoqi L, Weitao J. A multi-focus image fusion algorithm based on an improved dual-channel PCNN in NSCT domain. *Optik Int J Light Electron Opt*. 2013; 124(20):4104–9.
- [26] Das S, Kundu MK. NSCT-based multimodal medical image fusion using pulse-coupled neural network and modified spatial frequency. *Med Biol Eng Comput*. 2012; 50(10):1105–14.
- [27] Kong WW. Multi-sensor image fusion based on NSST domain FCM. *Electron Lett*. 2013; 49(13):802–3.
- [28] Kong W, Liu J. Technique for image fusion based on nonsubsampling shearlet transform and improved pulse-coupled neural network. *Opt Eng*. 2013; 52(1):017001.
- [29] Kong W, Zhang L, Lei Y. Novel fusion method for visible light and infrared images based on NSST–SF–PCNN. *Infrared Phys Techn*. 2014; 65:103–12.
- [30] Baum KG, Schmidt E, Rafferty K, Krol A, Helguera M. Evaluation of novel genetic algorithm generated schemes for positron emission tomography (PET)/magnetic resonance imaging (MRI) image fusion. *J Digit Imaging*. 2011; 24(6):1031–43.
- [31] Baum KG, Helguera M, Krol A. Fusion viewer: a new tool for fusion and visualization of multimodal medical data sets. *J Digit Imaging*. 2008; 21(1):59–68.
- [32] Tu T-M, Su S-C, Shyu H-C, Huang PS. A new look at IHS-like image fusion methods. *Inform Fusion*. 2001; 2(3):177–86.
- [33] He C, Liu Q, Li H, Wang H. Multimodal medical image fusion based on IHS and PCA. *Procedia Eng*. 2010; 7:280–5.
- [34] Daneshvar S, Ghassemian H. MRI and PET image fusion by combining IHS and retina-inspired models. *Inform Fusion*. 2010; 11(2):114–23.
- [35] Rudeman DL, Cronin TW, Chiao C-C. Statistics of cone responses to natural images: implications for visual coding. *J Opt Soc Am A*. 1998; 15(8):2036–45.
- [36] Reinhard E, Adhikhmin M, Gooch B, Shirley P. Color transfer between images. *IEEE Comput Graph*. 2001; 21(5):34–41.
- [37] Ganasala P, Kumar V. CT and MR image fusion scheme in nonsubsampling contourlet transform domain. *J Digit Imaging*. 2014; 27(3):407–18.
- [38] Xydeas CS, Petrovic V. Objective image fusion performance measure. *Electron Lett*. 2000; 36(4):308–9.
- [39] Piella G, Heijmans H. A new quality measures for image fusion. *Conf Proc IEEE Image process*. 2004; 3:173–6.